

Effect of various alkalis on hydration properties of alkali-activated slag cements

Shuhua Liu¹ · Qiaoling Li¹ · Weiwei Han¹

Received: 26 March 2017 / Accepted: 28 October 2017 / Published online: 11 November 2017
© Akadémiai Kiadó, Budapest, Hungary 2017

Abstract The effect of sodium silicate (NS system) and sodium hydroxide (NH system) on hydration properties of alkali-activated slag (AAS) cements is investigated, and more attention has been paid to the hydration kinetics in this paper. The increase of Na₂O dosage tends to promote higher early strength of the cements, but lower strength gain at later, while increasing SiO₂ dosage leads to improve both early and later strength. The hydration of the two AAS cements proceeds through three processes after induction period finished, namely nucleation and crystal growth (NG), phase boundary reaction (I), and diffusion (D). With the increased Na₂O dosage and decreased SiO₂ dosage, the NG and I processes are shortened. The hydration rate during NG and I processes is also accelerated. CSH gel is the main hydrates of all AAS cements, but the activator type and content have impact on the minor hydration products.

Keywords Alkali-activated slag cements · Hydration properties · Hydration heat · Hydration kinetics

Introduction

AAS cement is a mix of 100% ground granulated blast-furnace slag (GGBS, hereafter slag) with alkaline activators, of which slag is industrial by-products with latent hydraulicity, and can achieve high strength in the presence

of proper alkaline activator [1–3]. The alkaline activator, typically sodium hydroxide (NaOH), sodium silicate (often used in practice in the form of Na₂O·nSiO₂ or its mix with NaOH), is the well-known method to activated the hydraulic properties of slag [4–7].

Plenty of early studies have discussed the effect of activator type and content on the hydration kinetics of slag, concluding that early hydration of slag activated by both alkalis stated above proceeds in five stages, viz. pre-induction, induction, acceleration, deceleration, and diffusion, which is known to be a typical pattern for the hydration kinetics of OPC. But the hydration mechanism, the duration and intensity of each stage are distinct, depending on the type and concentration of the activator [8–11]. For sodium hydroxide-activated slag (NH) cements, its duration of each stage is very short, and no noticeable induction period is observed compared to OPC. But, for the sodium silicate-activated slag (NS) binders, it usually involves an initial double peak during the pre-induction stage and extended induction period, also, these two initial double peaks may merge into one depending on the prime materials used and the curing conditions [4, 5, 12–16]. A few recent studies, however, have noticed two dominant periods and three exothermic peaks in NS system, which is probably because the occurrence of new reaction processes of slag via a diffusion mechanism [4, 7].

With respect to activator content, Krizan and Zivanovic [13] discussed the effect of activator dosage on the hydration kinetics of sodium silicate-activated cements. An increment of activator dosage tends to accelerate the hydration rate and enhance both the initial and accelerated peak. Besides, the cumulative heat of hydration also increases but still lower than that of OPC. The results are in agreement with that reported by Gebregziabihier et al. [4], who have also studied the effects of the molarity of NaOH

✉ Shuhua Liu
shliu@whu.edu.cn

¹ State Key Laboratory of Water Resources and Hydropower Engineering Science, Wuhan University, Wuhan 430072, China

activator and silica modulus M_s (M_s : molar ratio of $\text{SiO}_2/\text{Na}_2\text{O}$) of sodium silicate activator on the hydration kinetics of AAS cements: A higher NaOH molarity tends to accelerate early hydration, but decrease the total heat evolution thereby limiting the hydration degree of slags. Moreover, a retarding effect of SiO_2 on hydration process of NS, compared with NH and OPC, is observed, and this effect appears to be even more evident when silica modulus increases, but with no penalty in the total heat evolution thereby the hydration degree of slags.

However, the exact hydration mechanism that explains the reaction of the slag with an alkaline activator is not yet quite understood. Some authors have considered the hydration process of AAS to occur through a highly heterogeneous reaction [17, 18]. And this heterogeneous reaction of AAS has been reported to be governed by three mechanisms: (a) nucleation and growth of initial solid phases, (b) interactions at the boundaries of the phases formed, and (c) diffusion through hydration products layer [18–23]. Fernandez and Puertas [9, 18] have discussed the reaction mechanism of slag with an alkaline activator after the induction period by develop mathematical models of hydration kinetics through use of calorimetric data. The authors of their early work, which has taken account of the effect of activator dosage and curing temperature in the reaction kinetics, reveal that the mechanism explaining the alkaline activation of slag after the induction period is mainly diffusion, and the Jander equation [23] best fits the experimental results [9, 20]. Thereafter, their further work considers the effect of activator type in the kinetic studies, indicates that once the induction period has finished, the reaction of slag with various activator is governed by three mechanisms of nucleation, phase boundary interaction, and diffusion. The kinetic equations that best describe these three mechanisms happen to be as same with the Krstulovic–Dabic model, which is mainly used and valid for the kinetic studies of cement-based materials [18, 22].

Consensus related to the hydration products has achieved based on enormous studies [24–28] that calcium silicate hydrate (C–S–H), or with aluminium-substituted, is the main reaction product of AAS. It is accompanied by the formation of hydrotalcite-type phase whenever the alkaline solution is composed of just NaOH or mixed with $\text{Na}_2\text{O}\cdot n\text{SiO}_2$. However, important disagreement over the existential state of sodium remain exists. Some researchers [29, 30] have noticed the zeolites such as natrolite and gismondine, while others [24, 31, 32] have found that there is no sodium-based hydrated compounds (zeolites) exist, but the sodium is most likely inside the C–S–H gel with the replacement of Ca^{2+} by Na^+ , leading to the formation of C–(Na)–S–H. AFm-type phases have also been identified formed in AAS cements according to some researchers [33–36].

As stated above, the effects of sodium silicate and sodium hydroxide and their content on the hydration properties have been conducted intensively. However, the existing literature mainly focus on the effect of silica content (or silica modulus M_s , and M_s equal to zero for sodium hydroxide, otherwise for sodium silicate) by keeping the percent sodium oxide constant, or the effect of activator dosage by keeping the silica modulus fixed, while neglecting the effect of sodium oxide content on the alkaline activation of slags with constant silica. In addition, the studies over the kinetics modeling of alkaline activation process of AAS by means of calorimetric data are relatively limited, and the law control the hydration of AAS after induction period is turn out to be fairly different as the previous statements. Thus, in this paper, the effect of alkaline activators with various sodium oxide and constant silica content, and the opposite, on the hydration properties of AAS cements, are investigated but without consideration of the dosage of sodium silicate, which has been reported in somewhere else at length by other authors [7]. More attention is paid to the effects on the hydration kinetics as well as the kinetic model [18]. Based on the results, the early hydration mechanism controlling the alkaline activation of slag is also analyzed in detail. Other important hydration properties including hydration products and microstructure of cement pastes as well as mechanical strength are also investigated to elaborate the topic.

Experimental

Materials

Ground-granulated blast furnace slag (slag) compliant with requirement of Chinese national standard GB/T 18046-2000 is used as the raw materials. Meanwhile, the ordinary Portland cement (CEM I 42.5) that conforms to Chinese national standard GB175-2007 is served as a reference in this study. Chemical composition of OPC and GGBS with their specific surface area of around 400 kg/m^2 is given in Table 1.

With respect to alkaline activators, sodium silicate solution with modulus (M_s , molar ratio of $\text{SiO}_2\text{--Na}_2\text{O}$) of 3.3 and sodium hydroxide pellets of industrial grade was used. Four aqueous solutions of sodium silicate, with silica molarity (M) of 2.5 and 1.5 and sodium oxide molarity (M) of 2 and 1.5 (the expression of activator has referred to [26] which may provide an easy way to elaborate the effect of SiO_2 and Na_2O dosage on hydration properties in this paper), were prepared by mixing sodium hydroxide previously dissolved in water with sodium silicate in proper proportion, forming what is actually a compound solution of sodium hydroxide and sodium silicate. Also, the solution

Table 1 Chemical composition of raw materials/mass, %

Raw materials	SiO ₂	Al ₂ O ₃	CaO	Fe ₂ O ₃	MgO	SO ₃	K ₂ O	Na ₂ O	P ₂ O ₅
OPC	19.59	5.64	62.63	3.61	1.52	3.50	0.82	0.12	0.12
GGBS	32.54	14.14	41.07	0.45	6.03	3.45	0.68	0.36	0.05

Table 2 Composition of activators with respect to 1 kg GGBS

AAS	SiO ₂ /M	Na ₂ O/M	Ms	H ₂ O(g)
NS-1	2.5	2	1.25	400
NS-2	1.5		0.75	400
4 M-NH	0		0	400
NS-3	2.5	1.5	1.67	400
NS-4	1.5		1	400
3 M-NH	0		0	400

with silica molarity equal to zero has been prepared by using NaOH alone, of which the actual concentration of NaOH equal to 4 and 3 M in correspond to 2 and 1.5 M Na₂O, respectively. The compositions of activators are summarized in Table 2.

Experimental methods

According to the mix proportion of the pastes shown in Table 3, 40×40×40 mm cubic specimens were prepared by the paste mixer with water to cement ratio of 0.4. All the specimens were cured in ambient environment with relative humidity (RH) higher than 90% and temperature of 20 ± 2 °C till the stipulated age of 3, 7, 28, and 90 days. The compressive strength of paste at different ages was tested by WAY-2000, an electro-hydraulic compression-testing machine. Specific test procedure is referred to GB/T 17671-2005: Method of Testing Cement-Determination of Strength.

And then, the specimens were broken, and the small samples in the central part of the specimens were selected to soak in anhydrous ethanol to terminate the hydration for microstructural tests of scanning electron microscopy

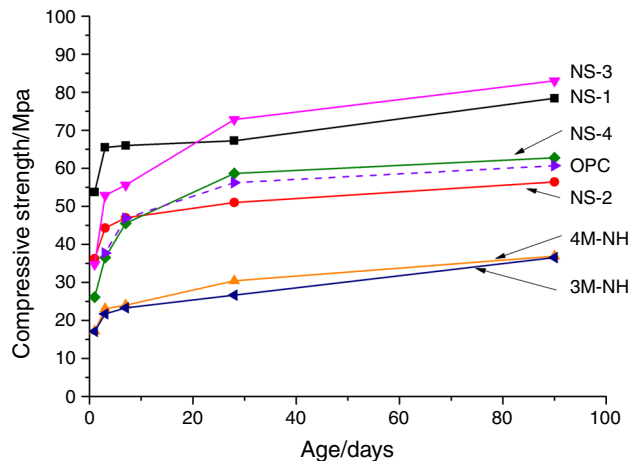


Fig. 1 Compressive strength of AAS cements

(SEM). The rest of sample pieces were ground in the agate mortar and dried in 60 °C for 2 h for X-ray diffraction (XRD) tests. The SEM equipment, used for hydrates morphology analysis, is JSM-5610LV produced from Japanese Electronics Co., Ltd. The XRD is detected by X’Pert Pro, Palytical of The Netherlands, with operating voltage of 40 kV and working current of 40 mA, setting the scanning scope ranging from 10° to 70° and scanning speed of 6° min⁻¹. The XRF experiments were measured on Axios advanced X-ray fluorescence instrument, in voltage range from 30 to 60 kV, with approximately 5 g of sample. The rates of heat evolution and the hydration heat release of all pastes with same water to cement ratio 0.4 were determined by a typical ex situ isothermal conduction calorimeter (Toni DCA7338), and the dosage is 10 g with accuracy 0.001 g.

Table 3 Kinetic parameters determined by means of the Knudsen extrapolation model

Sample	n	K ₁ ’	K ₂ ’	K ₃ ’	α ₁	α ₂	α ₁ - α ₂	Q _{max} ’
NS-1	1.6944	0.0689	0.0179	0.0035	0.1595	0.2626	0.1031	190.48
NS-2	1.7593	0.0868	0.0198	0.0032	0.1209	0.2226	0.1017	182.12
NS-3	1.5132	0.0373	0.0109	0.0026	0.2219	0.3526	0.1307	139.86
NS-4	1.5824	0.0534	0.0161	0.0037	0.2007	0.3245	0.1238	153.16
NH-1	1.2600	0.1426	0.0262	0.0043	0.0769	0.2258	0.1489	204.082
NH-2	1.2496	0.0914	0.0248	0.0041	0.1113	0.2331	0.1218	193.424

Results and discussion

Compressive strength

The compressive strength of all specimens measured at the stipulated age of 1, 3, 7, 28, and 90 days is presented in Fig. 1. The results indicate clearly that all cements show progressive strength development during curing ages. It is clearly that NHs exhibit the lowest compressive strength while NSs, of which the Na_2O concentration is same as NHs, present compressive strengths close to or even higher than that of OPC at corresponding age. In addition, the compressive strength is increasing with an increase of SiO_2 molarity in NSs with both 2 M Na_2O (NS-1 and NS-2) and 1.5 M Na_2O (NS-3 and NS-4). However, with regard to NSs with controlled SiO_2 concentration of 2.5 M (NS-1 and NS-3) or 1.5 M (NS-2 and NS-4), the compressive strength increases with the increase of Na_2O concentration at early age but just the opposite at later age. While for NHs, the strength development of NHs with lower molarity (3 M-NH) is slightly slower than the one with higher molarity (4 M-NH) before 28 days, but the strength of former catches up with that of the later at the age of 90 days.

Hydration heat evolution

Rate of heat evolution

The rate of hydration heat curves of AASs discussed in this paper is illustrated in Figs. 2–4. In all of these figures, OPC has been set as the control.

Figures 2 and 3 describe the hydration heat evolution rate of NS system, from which an obvious early exothermic peaks corresponding to initial dissolution and wetting of slag particles occurs during the first several minutes upon

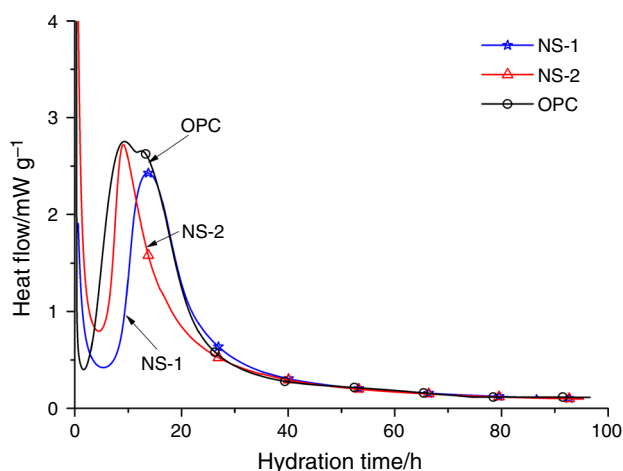


Fig. 2 Heat evolution rate of NSs with 2 M Na_2O

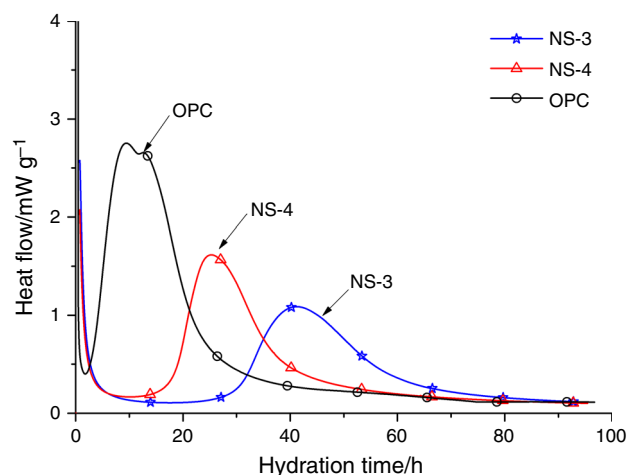


Fig. 3 Heat evolution rate of NSs with 1.5 M Na_2O

contact of slag with sodium silicate solution [4, 13, 23], followed by a long induction period and thereafter entering into acceleration period, which can be assigned to the substantial formation of CSH with various levels of metal ions (Ca, Na, Mg, etc.) substituted [5, 37–39]. As SiO_2 molarity increases, the induction period is prolonged and the signal of the second peak is less intense and delayed, which further demonstrates that SiO_2 has a retarding effect on the hydration of slag [4]. This retarding effect may be explained by the reasons that the hydrolyzation rate of OH^- from Na_2SiO_3 is inhibited with the increase of SiO_2 , leading to slower dissolution of slag and a decrease of relative Ca^{2+} concentration in the system [40–42]. Afterward, the time when Ca^{2+} reaches supersaturation is delayed, and the reaction between Ca^{2+} and $[\text{SiO}_4]^{4-}$ is decelerated and weakened.

Comparing Figs. 2 with 3, the hydration of slag is greatly accelerated with the increased Na_2O concentration. The induction period, which lasts nearly 30 h and 17 h at 3.7% Na_2O (NS-3 and NS-4), is reduced to 6 and 8 h (NS-1 and NS-2), respectively. In addition, the magnitude of accelerated hydration peak of NSs with 2 M Na_2O is higher than that with 1.5 M Na_2O and even comparable to that of OPC. These did indicate an acceleration effect of OH^- on the dissolution and hydration of slag.

Figure 4 represents the hydration heat evolution rate of NH system. For the NHs, there is no distinct induction period and dissolution period observed in the curves. Only one major peak is identified in the calorimetric data for both concentration of activators, which happens immediately after mixing the slag with NaOH solution. This may ascribe to rapid hydration rate caused by high OH^- concentration in the solution, leading to the dissolution and induction period occurring within around a few minutes or less and even not possible to be detected. The hydration of NHs proceeds so quickly compared with that of NSs, the

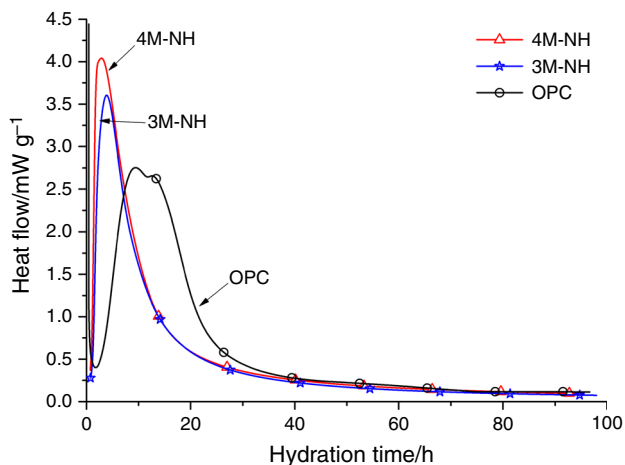


Fig. 4 Heat evolution rate of NHs

hydration rate and the magnitude of second peak even exceed that of OPC. The acceleration period corresponding to the substantial formation of CSH is advanced slightly, and the intensity of the second peak is also enhanced mildly with increased Na₂O concentration or NaOH molarity.

hydration heat

The cumulative hydration heat curves of all AASs are shown in Figs. 5–7. From these figures, lower total heat evolution of AAS systems than OPC is observed, which may contribute to the extensive use for engineering practice.

Figures 5 and 6 show the cumulative heat evolution of NSs decreases disproportionately with the increase of SiO₂ molarity, indicating a higher hydration degree of slag with lower SiO₂ molarity. The compressive strengths of NSs, however, increase proportionally with the increase of silica

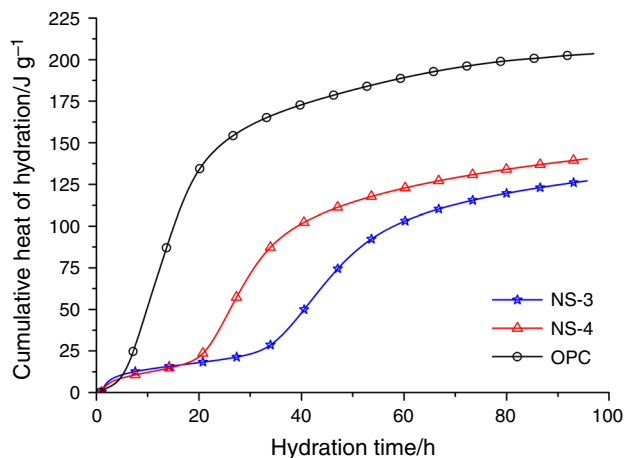


Fig. 6 Hydration heat of NSs with 1.5 M Na₂O

molarity. As increasing silica indicates more [SiO₄]⁴⁻ but less OH⁻ hydrolyzed from sodium silicate in the solution. On the one hand, an increase of [SiO₄]⁴⁻ contributes to the formation of CSH with increased quantity and polymerization degree. On the other hand, the less OH⁻ results in decreased hydration degree of slag [6, 7, 13, 29]. When the contribution of the former outweighs the negative impact of the later, the reason that the compressive strength increases with increased silica is explained.

Comparing Figs. 5 with 6, the cumulative heat evolution is greater with higher Na₂O dosage, implying a higher hydration degree with increased Na₂O. This follows well with the early age strength development discussed in the previous section, i.e., the higher the Na₂O dosage, the higher the early strengths. However, this relationship between strength and Na₂O dosage is inverted at late curing ages (after 28 days), it may be attributed to the reason that higher OH⁻ initiates the hydration process more quickly and results in a faster and denser early product

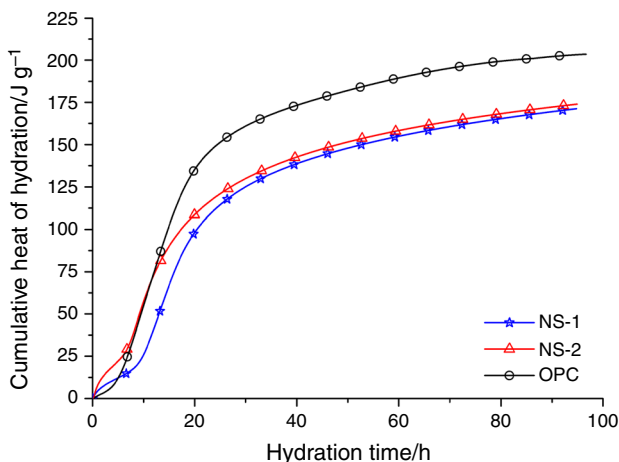


Fig. 5 Hydration heat of NSs with 2 M Na₂O

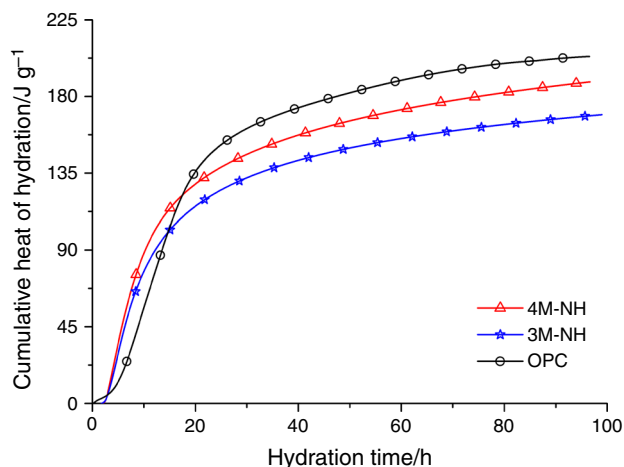


Fig. 7 Hydration heat of NHs

formation, thus limiting the later-age microstructural development and strength gain. Furthermore, it worth to be noted that the cumulative heat evolution and consequent hydration degree of NSs with higher Na₂O are greater than the one with lower Na₂O, the compressive strength, however, seems to depend more on the SiO₂ concentration, and the more the SiO₂ molarity, the higher the strength. For instance, the strength of NSs with higher silica molarity (NS-1 and NS-3) is shown to be much higher than the one with lower silica molarity (NS-2 and NS-4). This may indicate that the strength relies more on the reaction of [SiO₄]⁴⁻ clusters and structural development than on the hydration degree.

Figure 7 presents the cumulative heat evolution curves of NHs. It is observed that increasing activator molarity of NaOH results in greater cumulative heat evolution and therefore a higher degree of hydration, which is consistent with the strength in the previous section that the early compressive strength of 4 M-NH is higher than that of 3 M-NH as a whole. But the strength development of 4 M-NH after 28 days is slower than that of 3 M-NH. This results, combined with the effect of Na₂O content on the strength of NSs as stated above, indicate that a higher Na₂O is unfavorable to the long-term strength development.

Comparing the hydration heat evolution of NHs and NSs with their strength. It is evident that NHs display faster hydration rate and hydration degree but relatively lower compressive strengths than NSs, since the C-S-H formed using NaOH at early ages is denser and less porous, and the further hydrates are formed mainly in the place of original slag particle but not in the empty coarse pores, leading to lower compressive strength even with higher degree of hydration compared to NSs [24], which again indicates that the strength development relies more upon the reaction of ion cluster and the microstructural development than upon the hydration degree.

Hydration process simulation

Kinetic model

The Krstulovic–Dabic model assumed that three basic processes taking place in a heterogeneous system, namely nucleation and crystal growth (NG), phase boundary interaction (I), and diffusion (D) [22], which has also been reported to be reaction processes occur in alkaline activated slag as previously mentioned. All the three processes are considered to occur simultaneously but the one with the lowest rate dominates the hydration process as a whole [41]. The Krstulovic–Dabic model provides the basic kinetic equations describing the three dominating processes. Among those equations, the basic Avrami–Erofeev Eq. (1) is taken to describing hydration kinetics during the

dominate nucleation and growth process [43], Eq. (2) is usually used for interactions at phase boundaries, and Jander's Eq. (3) is the best to explain this diffusion process [23].

$$[-\ln(1-\alpha)]^{1/n} = K_1 r^{-1}(t-t_0) = K'_1(t-t_0) \quad (1)$$

$$[1-(1-\alpha)^{1/3}] = K_2 r^{-1}(t-t_0) = K'_2(t-t_0) \quad (2)$$

$$[1-(1-\alpha)^{1/3}]^2 = K_3 r^{-2}(t-t_0) = K'_3(t-t_0) \quad (3)$$

where α is hydration degree; $K_1(K'_1)$, $K_2(K'_2)$, $K_3(K'_3)$ are rate constant corresponding to three hydration process of NG, I, and D; t is hydration time; t_0 is the ending time of induction period; n is the crystal growth index reflects the geometrical crystal growth, $1 \leq n \leq 2$ [28]; r is the particle radius.

When α is differentiated with respect to t in the equations above, hydration rate of each process of NG, I, and D is obtained the equations being as follows:

$$d\alpha/dt = F_1(\alpha) = K_1(1-\alpha)[- \ln(1-\alpha)]^{(n-1)/n} \quad (4)$$

$$d\alpha/dt = F_2(\alpha) = 3K_2(1-\alpha)^{2/3} \quad (5)$$

$$d\alpha/dt = F_3(\alpha) = 3/2[K_3(1-\alpha)^{2/3}]/[1-(1-\alpha)^{1/3}] \quad (6)$$

where $F_1(\alpha)$, $F_2(\alpha)$, and $F_3(\alpha)$ represent the hydration process of NG, I, and D, respectively. Based on the hydration heat values $Q'(t)$ and the rate of hydration evolution dQ/dt obtained through isothermal conduction calorimetry, the hydration degree α and hydration rate $d\alpha/dt$ required for the kinetic simulation of hydration process are determined by the following equations [44].

$$\alpha(t) = Q'(t)/Q'_{\max} \quad (7)$$

$$d\alpha/dt = dQ/dt \cdot \frac{1}{Q'_{\max}} \quad (8)$$

where this newly defined $Q'(t)$ is the heat released from the end of induction period due to the fact that the dissolution period progress so fast that it is not always possible to be detected, meanwhile, the induction period is also considered to make a small contribution to the total heat. So, this simulation is conducted from the beginning of the second peak, namely the ending of the induction period [9]; Q'_{\max} is the total heat released when the reaction has completely finished and is obtained by using the Knudsen extrapolation Eq. (9) to linear fit the hydration heat evolution curves [18]:

$$\frac{1}{Q'} = \frac{1}{Q'_{\max}} + \frac{t_{50}}{Q'_{\max}(t-t_0)} \quad (9)$$

where t_{50} is the time required for releasing 50% of the total heat.

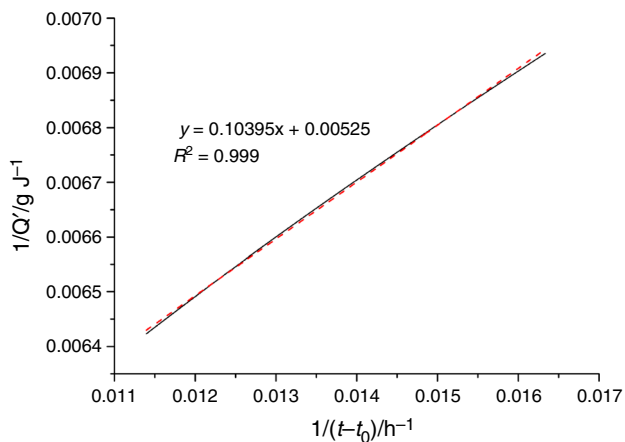


Fig. 8 Determination of maximum hydration emission heat Q'_{max} from linear regression

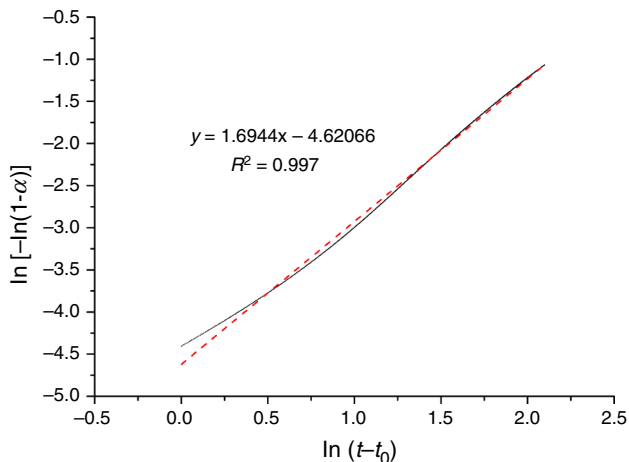


Fig. 9 Determination of kinetic factors (n and K'_1) of nucleation and crystal growth (NG) process from linear regression

For a real system, the Q'_{max} is firstly calculated by taking Eq. (9) to linear fit the hydration heat data of AASs, as shown in Fig. 8. Kinetic parameters K'_1 and n under NG process would be deduced and calculated by Eq. (4), as shown in Fig. 9. K'_2 under process I and K'_3 under process D would be deduced and calculated by using the same method.

Then by substituting those parameters into Eqs. (4)–(6), the kinetic curves $F_1(\alpha)$, $F_2(\alpha)$, and $F_3(\alpha)$ as a function of degree of hydration α are procured. Likewise, the experimental curves of hydration rate ($d\alpha/dt$) as a function of α are also obtained by Eq. (8). Finally, a comparison of the simulated curves with the experimental curves of hydration rate and an analysis of the kinetic parameters is performed to understand the reaction mechanism controlling the alkaline activation process of slag.

Determination of hydration mechanism

As shown in Fig. 10, theoretical curves $F_1(\alpha)$, $F_2(\alpha)$, and $F_3(\alpha)$ simulated by Krstulovic–Dabic model are compared with practical hydration rate ($d\alpha/dt$) curves deduced from experimental data. It can be seen in Fig. 10 that the hydration rate curves $d\alpha/dt$ could be well segmentally simulated by theoretical curves $F_1(\alpha)$, $F_2(\alpha)$, and $F_3(\alpha)$. It also deduced that all activated-slag involves three processes of NG, I , and D when the induction period has finished.

In the early hydration of sodium silicate-activated slags (Fig. 10a–d) after induction period, a nucleation and crystal growth dominate the hydration process because of the sufficient alkaline solution supply and deficient hydration products [24, 47]. The NG process involves the formation of nuclei and the growth of hydrate phase from a fixed nuclei when a stable supersaturation of Ca^{2+} dissolved from slag grain is maintained [48, 49]. However, there were disagreements over the manner of nucleation and growth process. Some authors [7, 13, 24] hold that the NG process of NSs is a heterogeneous reaction and occurs preferentially on the surface of the grains, and hydration products grow outward from the grain into the capillary pore space, which is consistent with that in OPC or C_3S . Whereas other authors [10, 45] claim that hydrates formation occurs by nucleation in the capillary space away from the grain surface through a homogeneous “through solution” process as they mention the observation of a fast formation of a gel-like interstitial matrix but no reaction rim around the slag grain. Nonetheless, as shown in Fig. 10, the NG process is fitted by kinetic models with high relevancy. It combines with the fact that the heterogeneous process has lower activation energy than homogeneous nucleation, and indicates the nucleation occurs on solid surface preferentially through a heterogeneous nucleation process [13, 14]. Thereafter, if the nuclei of the products formed in NG process are uniformly distributed on the solid surface and with the continuous growth of the hydrated phase, the reacting interphase between solid surface and pore solution is rapidly formed; in this stage, the phase boundary reaction governs the hydration process. With hydration process continues, the hydration process is thereafter governed by the diffusion owing to a relative large amount of hydration products formed and a lack of water for ion migration [38].

For the hydration kinetics of NaOH-activated slag (Fig. 10e–f), it is also deduced that the process of alkaline activation of slag goes through nucleation and crystal growth once the induction period has finished, but may be a continuing NG process as the pre-induction stage may involve substantial initial product formation according to some researches [4, 5, 24]. With prolonged hydration process, the hydration turns to I stage and then turns to

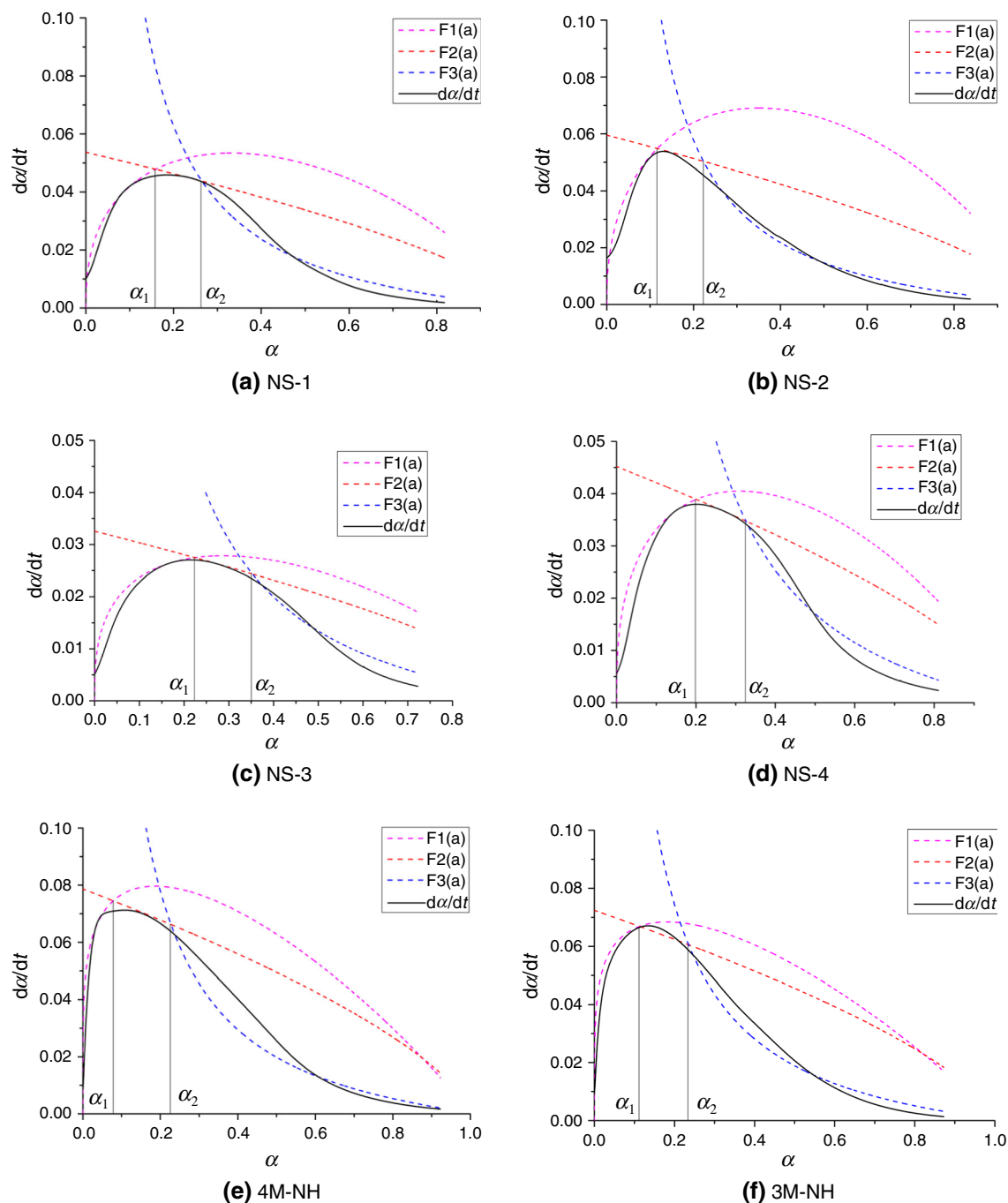


Fig. 10 Hydration rate curves for **a** NS-1; **b** NS-2; **c** NS-3; **d** NS-4; **e** NH-1; **f** NH-2

D stage because of space restrictions and the lack of availability of water, which cause the ion migration to be relatively difficult.

Kinetic parameters analysis

The kinetic parameters of hydration process of AAS are shown in Table 3. A comparison of kinetic parameters for the samples indicates essential differences in the system

[24]. The values of exponent n , which describes nucleation and the geometrical crystal growth [34], increase with increased dosage of Na_2O and decrease with increased SiO_2 molarity for all examined AAS cements. This indicates that the activator type and content have pronounced effect on the crystal growth geometry.

It can be seen in Table 3 that the rate of NG process is about 4–5 times the rate of *I* process, and it is about 20 times the rate of *D* process for NS system. And, for NH

system, the difference in rate between NG process and *D* process is even large, which implies that the hydration rate of NG process is the fastest followed by that of *I* and *D* process in sequence. The hydration of slag in the presence of alkaline activator during NG process is the autocatalytic reaction. Owing to the fairly high concentration of alkaline solution and a relatively small number of hydration products formed at the initial period, it provides a strong driving force for forming a dispersive phase of crystal nucleus on the active centers of slag and also exerts a significant crystallization pressures for the growth of these crystal nucleus [29, 30]. In addition, the continuous growth of the crystal nucleus leads to an increase in their area of boundaries, which in turn accelerate the autocatalytic reaction. Thus, the hydration reaction during NG process is fairly fast. Nevertheless, the rate of phase-boundary reaction is affected by the ion concentration, the surface area of the crystal, growth space of hydration products, etc. [46]. Due to the fact, the NG process, during which the products formation is accelerated, has consumed a great deal of reactive ion and occupies a lot of space, thus the reaction rate on the reacting interphase between pore solution and solid surface of slag during *I* process may be lower than the reaction rate during NG process. When the reaction proceeds into *D* process, the hydration reaction becomes even slower because of the lower concentration of alkaline solution, the less growth space for hydration products as well as the continual thickening of the products, which makes the ion mobility even more difficult. As shown in Table 3, for NS system, the value of K'_1 increases with increasing concentration of Na_2O , but decreases with an increase of SiO_2 molarity. The increase of Na_2O concentration and the drop of SiO_2 molarity lead to the increase in OH^- thus an increase in the growth rate of crystal nucleus. As a result, the rate of hydration reaction during NG process is accelerated with increasing Na_2O concentration but decreasing SiO_2 molarity. For *I* process, the values of K'_2 basically obey the same regularity as K'_1 . Owing to the faster hydration reaction during NG process with higher OH^- , a greater concentration of dissolved ions and an increase of area of phase boundary between crystals and pore solution may be obtained, thus, the rate of hydration reaction during *I* process is also accelerated. K'_3 , however, displays irregularity for NSs and seems to be influenced by both the activator content and the products formed during NG and *I* process [38, 40]. When activated with NaOH, the rate of hydration, K'_1 , K'_2 and K'_3 all increase compared with that of NS system and all increase with increasing Na_2O dosage. This is due to the greater driving force of high OH^- concentration for the dissociation of slag grains and acceleration of the hydration reaction by providing an alkaline environment. Additionally, more hydration

products formed in NS than in NHs because of the presence of additional $[\text{SiO}_4]^{4-}$ from sodium silicate [13], hindering the transport of reactants. It indicates that the type and content of activator greatly affect the hydration process of slag.

The intersection points of the curves, namely α_1 and α_2 , which are turning point from NG to *I* and *I* to *D*, respectively, are also given in Table 3. With respect to NS system, it is clear that both of duration for the NG process and *I* process are shortened with increasing Na_2O concentration and decreasing SiO_2 molarity; namely, the increasing of Na_2O promotes the hydration reaction of samples to transform from NG to *I* process and from *I* process to *D* process at a relatively low degree of hydration. This is probably due to the reason that a higher concentration of Na_2O plus a lower SiO_2 molarity in alkaline solution is conducive to hydrolyzing more OH^- , which will greatly promote the early hydration of NG and *I* process, leading to a shaper exothermic rate peak and shorter hydration duration [29]. Thus, the transformations occur at a relatively

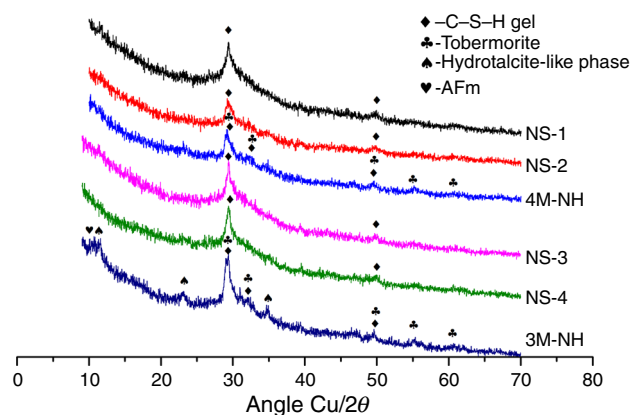


Fig. 11 XRD analysis of AAS pastes at age of 28 days

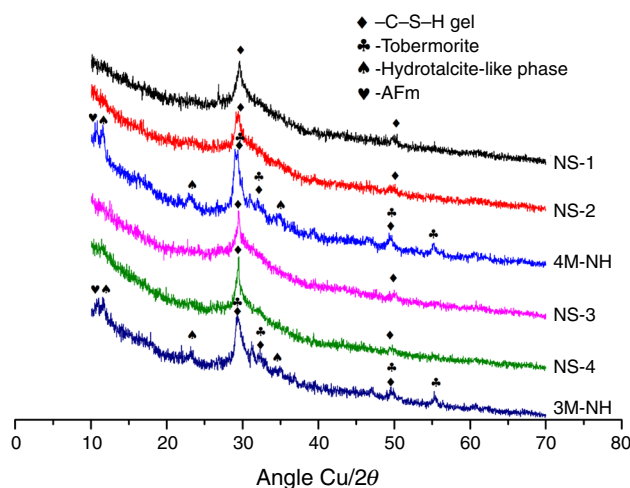


Fig. 12 XRD analysis of AAS pastes at age of 90 days

lower degree. The same trend for NHs by increasing Na_2O molarity is also identified with the similar reasons.

Hydration products

XRD

Figures 11 and 12 show the XRD patterns of AAS pastes at 28 and 90 days, respectively. For all hydrated samples, a obvious diffraction peak at $29^\circ 2\theta$ and a less evident reflection at $49.5^\circ 2\theta$ are observed, which can be attributed to C-S-H (PDF 033-0306) [24]. The diffraction peak at $29^\circ 2\theta$, combined with that at $23^\circ 2\theta$, could also be partly due to calcite resulting from carbonation. In the NaOH activated system, an additionally reflection at $7^\circ 2\theta$ (not showing here as curves before $2\theta = 10^\circ$ has been cut off for layout aesthetics) is detected and also a less broad reflection at $29^\circ 2\theta$ that match with the powder diffraction file of C-S-H(I) (PDF 034-0002) [29]. This phase can also be identified at $32^\circ 2\theta$, $50^\circ 2\theta$, and $55^\circ 2\theta$, which indicates that hydration products formed in NHs are more highly crystalline than those formed in NSs. Besides, reflections at $11^\circ 2\theta$ and $23^\circ 2\theta$ corresponding to hydrotalcite-like

phase (PDF 043-0072) can also be detected in NH-2 but not in NH-1 at 28 days. This may due to the non-uniform sampling process according to the following SEM analysis. In addition, the XRD patterns at curing age of 90 days show that the type of the hydration products of AASs, especially for NHs, is much the same with that at the age of 28 days except that the quantity of hydration products has improved, indicating a stable phase change in the later stage.

Sem

The SEM micrographs of AAS pastes at 28 and 90 days are presented in Figs. 13 and 14, respectively, which confirmed that the gel-like phase of calcium silicate hydrate (C-S-H gel) is main hydration products of alkali activation of GGBS whenever the alkaline solution was composed just of sodium hydroxide or mixed with sodium silicate [24, 25]. At the same time, the SEM micrographs clearly reveal the presence of typical hexagonal lamellar calcium hydroxide (CH) embedded in or interspersed in the calcium silicate hydrate gel structures in both NS and NH systems. Peaks expected for this phase, however, are difficult to distinguish in the XRD patterns, which may be

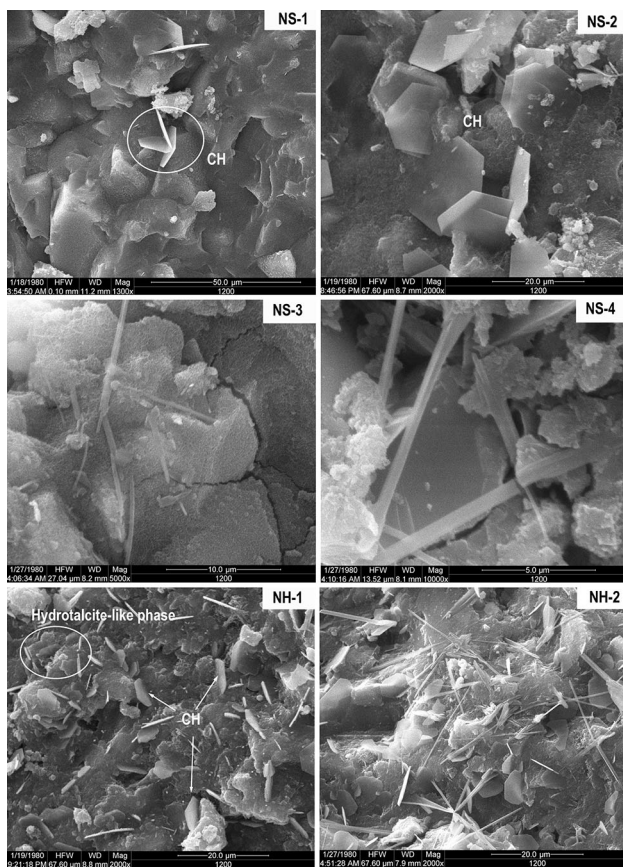


Fig. 13 SEM micrographs of AAS pastes at age of 28 days

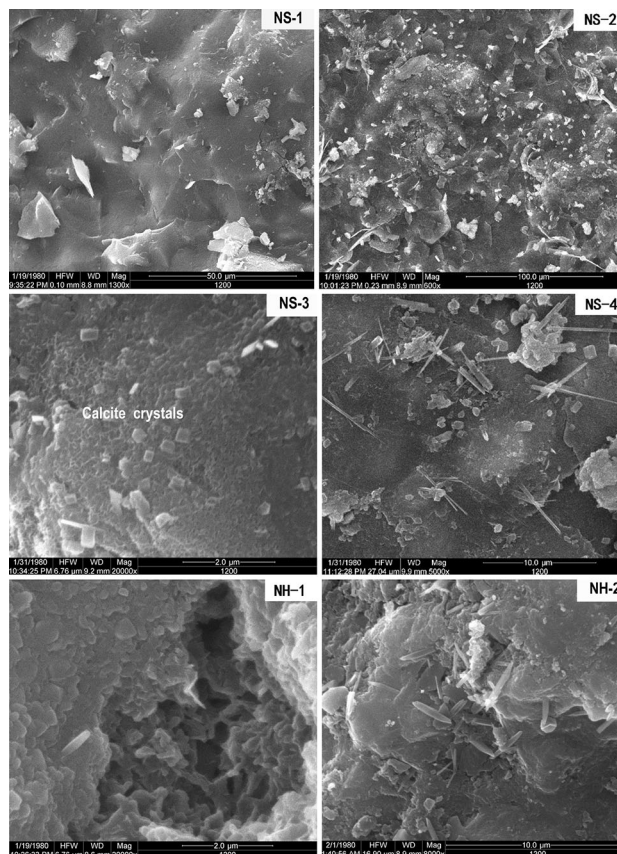


Fig. 14 SEM micrographs of AAS pastes at age of 90 days

attributed to the carbonization that translate CH into CaCO_3 . Lamellar hydrated phase can also be observed in NH system, which may be attributed to hydrotalcite-like phase. And it verifies the results of XRD. Needle or rod-like phase is also observed present on the C–S–H plane; this is probably AFm-type phase according to the XRD results. Compare Figs. 9 with 8, the microstructure of NS pastes at 90 days becomes much denser than that at 28 days. It is observed that most of the flake-like or rod-like hydrated phase is nearly wrapped by calcium silicate gel and just a small amount randomly distributed on fracture surface. This results in an increment in the strength at later. And the rhombohedral calcite crystals, which seem to be inconspicuous at early curing age of 28 days, appear in large numbers on the fracture surface. This may attribute to the carbonization of CH as well as C–S–H. Moreover, the microstructure of NH pastes seems to be looser than that of NS pastes, which may explain the lower strength of NHs compared to NSs.

Conclusions

The conclusions can be summarized as follows:

- (1) For both activators (the SiO_2 molarity of NaOH can be considered zero), the increase of the SiO_2 concentration, which indicates higher $[\text{SiO}_4]^{4-}$ concentration, leads to the improved early- and later-age strength, but has a retarding effect on early-age hydration and reduces the total heat evolution thereby the hydration degree of slag. While increasing the concentration of Na_2O , which indicates higher $[\text{OH}]^-$ concentration, results in accelerated hydration rate, higher total heat evolution thereby higher hydration degree of slags, higher early-age strength but lower strength gain at later-age. NHs display faster hydration rate and hydration degree but relatively lower compressive strengths than NSs. The strength development relies more upon the reaction of ion cluster and structural development than upon the hydration degree to some extent.
- (2) Hydration of the both kinds of AAS cements, after induction period finished, proceeds through three processes, namely nucleation and crystal growth (NG), phase boundary reaction (*I*), and diffusion (*D*). With the increased Na_2O and decreased SiO_2 dosage, which denotes more OH^- , the NG and *I* processes are shortened. Besides, the hydration rate of NG and *I* process calculated by the kinetics model is also accelerated, which is consistent with the experimental heat evolution data. The rate of hydration for *D* process, however, seems to be influenced by both the activator type and content, and the products formed during NG and *I* process.
- (3) CSH gel is identified to be hydration products of AASs regardless of the activator type and content. The SEM results indicate the generation of $\text{Ca}(\text{OH})_2$ in both systems. Based on XRD results, tobermorite and hydrotalcite-like phase as well as AFm-type phase are also detected in NH system but not in NS system.

Acknowledgements This Project is funded by the National Key R&D Program of China (2016YFC0401907) and the Opening Funds of Guangxi Key Laboratory of New Energy and Building Energy Saving (15-J-22-4-001).

References

1. Chi M, Huang R. Effects of dosage and modulus ratio of alkali-activated solution on the properties of slag mortars. *Adv Sci Lett*. 2012;16:7–12.
2. Palou MT, Kuzielová E, Žemlička M. Blended cements consisting of Portland cement–slag–silica fume–metakaolin system. *J Therm Anal Calorim*. 2016;125:1025–34.
3. Han F, Zhang Z, Wang D. Hydration kinetics of composite binder containing slag at different temperatures. *J Therm Anal Calorim*. 2015;121:815–27.
4. Gebregziabher BS, Thomas R, Peethamparan S. Very early-age reaction kinetics and microstructural development in alkali-activated slag. *Cem Concr Comp*. 2015;55:91–102.
5. Gebregziabher BS, Thomas RJ, Peethamparan S. Temperature and activator effect on early-age reaction kinetics of alkali-activated slag cements. *Constr Build Mater*. 2016;113:783–93.
6. Ravikumar D, Neithalath N. Effects of activator characteristics on the reaction product formation in slag cements activated using alkali silicate powder and NaOH. *Cem Concr Comp*. 2012;34:809–18.
7. Burciaga-Díaz O, Escalante-García JI. Structure, mechanisms of reaction, and strength of an alkali-activated blast-furnace slag. *J Am Cera Soc*. 2013;96:3939–48.
8. Zhou H, Wu X, Xu Z, Tang M. Kinetic study on hydration of alkali-activated slag. *Cem Concr Res*. 1993;23:1253–8.
9. Fernández JA, Puertas F. Alkali-activated slag cements: kinetic studies. *Cem Concr Res*. 1997;27:359–68.
10. Gruskovnjak A, Lothenbach B, Holzer L. Hydration of alkali-activated slag: comparison with ordinary Portland cement. *Adv Cem Res*. 2006;18:119–28.
11. Rashad AM, Bai Y, Basheer PAM. Hydration and properties of sodium sulfate activated slag. *Cem Concr Comp*. 2013;37:20–9.
12. Klemczak B, Batog M. Heat of hydration of low-clinker cements. *J Therm Anal Calorim*. 2016;123:1351–60.
13. Krizan D, Zivanovic B. Effects of dosage and modulus of water glass on early hydration of alkali–slag cements. *Cem Concr Res*. 2002;32(2002):1181–8.
14. Shi C, Day RL. A calorimetric study of early hydration of alkali-slag cements. *Cem Concr Res*. 1995;25:1333–46.
15. Chang JJ. A study on the setting characteristics of sodium silicate-activated slag pastes. *Cem Concr Res*. 2003;33:1005–11.
16. Fernández JA, Palomo G, Puertas F. Alkali-activated slag mortars: mechanical strength behaviour. *Cem Concr Res*. 1999;29:1313–21.

17. Bernal SA, Provis LJ, Rose V, Gutierrez RMD. Evolution of binder structure in sodium silicate-activated slag-metakaolin blends. *Cem Concr Comp*. 2011;33(2011):46–54.
18. Fernandez JA, Puertas F, Arteaga A. Determination of kinetic equations of alkaline activation of blast furnace slag by means of calorimetric data. *J Therm Anal Calor*. 1998;52:945–55.
19. Provis JLL, Deventer JS. Alkali activated materials. *RILEM State-of-the-Art Reports*. 2014; 13:339–379.
20. Fernández JA, Puertas F. Influence of the activator concentration on the kinetics of the alkaline activation process of a blast furnace slag. *Mater De Constr*. 1997;47:231–46.
21. Fernández JA, Puertas F. The alkali–silica reaction in alkali-activated granulated slag mortars with reactive aggregate. *Cem Concr Res*. 2002;32:1019–24.
22. Krstulović R, Dabić P. A conceptual model of the cement hydration process. *Cem Concr Res*. 2000;30:693–8.
23. Sun JY, Gu X. Study on hydration mechanism of slag activated by alkaline. *Adv Mater Res*. 2011;374:1582–8.
24. Haha MB, Saout GL. Influence of activator type on hydration kinetics, hydrate assemblage and microstructural development of alkali activated blast-furnace slags. *Cem Concr Res*. 2011;41:301–10.
25. Fernández JA, Puertas F, Sobrados I, Sanz J. Structure of calcium silicate hydrates formed in alkaline-activated slag: influence of the type of alkaline activator. *J Am Cera Soc*. 2004;86:1389–94.
26. Brough AR, Atkinson A. Sodium silicate-based, alkali-activated slag mortars: part I. Strength, hydration and microstructure. *Cem Concr Res*. 2002;32:865–79.
27. Wang SD, Scrivener KL. Hydration products of alkali activated slag cement. *Cem Concr Res*. 1995;25:561–71.
28. Escalante-García JI, Fuente AF, Alexer G, Fraire-Luna PE, Guillermo M. Hydration products and reactivity of blast-furnace slag activated by various alkalis. *J Am Cera Soc*. 2003;86:2148–53.
29. Zhang YJ, Zhao YL, Li HH, Xu DL. Structure characterization of hydration products generated by alkaline activation of granulated blast furnace slag. *Mater Sci*. 2008;43:7141–7.
30. Bernal SA, Gutierrez RMD, Provis JL, Rose V. Effect of silicate modulus and metakaolin incorporation on the carbonation of alkali silicate-activated slags. *Cem Concr Res*. 2010;40:898–907.
31. John VM. Blast furnace slag cements activated with waterglass. PhD thesis, Universidade of São Paulo, 1995.
32. Silva MG and Agopyan V. Hydration of blast furnace slag cements. Influence of temperature. *Tech. mag. BT/PCC/204*, University of São Paulo, 1998.
33. Gifford PM, Gillot JE. Alkali-silica reactions (ASR) and alkali-carbonate reaction (ACR) in activated blast furnace slag cement (ABFSC) concrete. *Cem Concr Res*. 1996;26:21–6.
34. Bonk F, Schneider J, Cincotto MA, Panepucci H. Characterization by multinuclear high-resolution NMR of hydration products in activated blast-furnace slag pastes. *J Am Cera Soc*. 2004;86:1712–9.
35. Chen W, Brouwers HJH. The hydration of slag, part 1: reaction models for alkali-activated slag. *J Mater Sci*. 2007;42:444–64.
36. Lothenbach B, Gruskovnjak A. Hydration of alkali-activated slag: thermodynamic modelling. *Adv Cem Res*. 2007;19:81–92.
37. Jansen D, Goetz-Neunhoeffer F, Lothenbach B, Neubauer J. The early hydration of ordinary Portland cement (OPC): an approach comparing measured heat flow with calculated heat flow from QXRD. *Cem Concr Res*. 2012;42:134–8.
38. Bullard JW, Jennings HM, Livingston RA. Mechanisms of cement hydration. *Cem Concr Res*. 2010;41:1208–23.
39. Han F, Zhang Z, Liu J. Hydration kinetics of composite binder containing fly ash at different temperatures. *J Therm Anal Calorim*. 2016;124:1691–703.
40. Thomas JJ, Biernacki JJ, Bullard JW, Bishnoi S, Dolado JS. Modeling and simulation of cement hydration kinetics and microstructure development. *Cem Concr Res*. 2011;41:1257–78.
41. Wang XY, Lee HS, Park KB, Golden JS. A multi-phase kinetic model to simulate hydration of slag–cement blends. *Cem Concr Comp*. 2010;32(2010):468–77.
42. Chang X, Yang X, Zhou W. Influence of glass powder on hydration kinetics of composite cementitious materials. *Adv Mater Sci Eng*. 2015;2015:1–7.
43. Bezjak A. Nuclei growth model in kinetic analysis of cement hydration. *Cem Concr Res*. 1986;16:605–9.
44. Schutter GD, Taerwe L. General hydration model for Portland cement and blast furnace slag cement. *Cem Concr Res*. 1995;25:593–604.
45. Hubler MH, Thomas JJ, Jennings HM. Influence of nucleation seeding on the hydration kinetics and compressive strength of alkali activated slag paste. *Cem Concr Res*. 2011;41:842–6.
46. Han F, Zhang Z, Liu M. Early hydration properties of composite binder containing limestone powder with different finenesses. *J Therm Anal Calorim*. 2016;123:1141–51.
47. Nath SK, Mukherjee S, Maitra S. Kinetics study of geopolymerization of fly ash using isothermal conduction calorimetry. *J Therm Anal Calorim*. 2017;127:1953–61.
48. Bullard WJ. Determination of hydration mechanisms for tricalcium silicate using a kinetic cellular automaton model. *J Am Cera Soc*. 2008;91:2088–97.
49. Bullard JW, Flatt RJ. New insights into the effect of calcium hydroxide precipitation on the kinetics of tricalcium silicate hydration. *J Am Cera Soc*. 2010;93:1894–903.